

# Femtosecond Dynamics of DNA Photolyase: Energy Transfer of Antenna Initiation and Electron Transfer of Cofactor Reduction

Chaitanya Saxena,<sup>†</sup> Aziz Sancar,<sup>‡</sup> and Dongping Zhong<sup>\*,†</sup>

Departments of Physics, Chemistry, and Biochemistry, OSU Biophysics, Chemical Physics, and Biochemistry Programs, 174 West 18th Avenue, The Ohio State University, Columbus, Ohio 43210, and Department of Biochemistry and Biophysics, Mary Ellen Johns Building, CB 7260, University of North Carolina School of Medicine, Chapel Hill, North Carolina 27599

Received: April 13, 2004; In Final Form: June 9, 2004

Photolyase is an enzyme that uses light energy to repair UV-induced DNA damage. We report here our femtosecond studies of the complex dynamics of energy and electron transfer in *E. coli* photolyase. Under physiological conditions, the excitation energy transfer from the antenna molecule methenyltetrahydrofolate (MTHF) to the fully reduced cofactor flavin (FADH<sup>-</sup>) occurs in 292 ps, but it takes 19 ps to the in vitro oxidized neutral cofactor (FADH). The orientation factors were found to be 0.11 for the MTHF–FADH<sup>-</sup> pair and 0.28 for MTHF–FADH, unfavorable for energy transfer, indicating the existing structural constraints probably placed by three functional binding sites. The photoreduction of the neutral FADH to the catalytically active cofactor FADH<sup>-</sup> was revealed to evolve along two electron-transfer pathways: one is along a tryptophan triad with the initial electron hop in 10 ps; the other route starts with an initial electron separation in 40 ps through the neighboring phenylalanine followed by either tunneling along an  $\alpha$ -helix or hopping through the tryptophan triad again. Reoxidation of the fully reduced flavin cofactor was observed to occur within  $\sim$ 4 ns in the presence of oxygen. These results reveal the ultrafast nature of the functional dynamics in photolyase and provide important dynamic information for further studies of mapping out the entire catalytic process of repairing damaged DNA.

## I. Introduction

Photolyase is one of a few photoenzymes existing in nature and performs the important biological function of repairing damaged DNA.<sup>1,2</sup> The function is triggered by the absorption of one photon, and thus the dynamics can be well synchronized with the functional process by a femtosecond laser pulse initiation. This enzyme has been considered to be a model system and has been the subject of many studies over the past two decades.<sup>2–10</sup> Various techniques<sup>11–18</sup> have been used to characterize the elementary reactions involved to elucidate the molecular mechanism of the catalytic process.

DNA photolyase from *E. coli* has been extensively studied,<sup>2</sup> and the X-ray structure at 2.3 Å has been reported.<sup>19</sup> The enzyme consists of a single polypeptide chain of 471 amino acids with two well-defined domains: an N-terminal  $\alpha/\beta$  domain (residues 1–131) and a C-terminal  $\alpha$ -helical domain (residues 204–471), which are connected to one another with a long interdomain loop (residues 132–203) that wraps around the  $\alpha/\beta$  domain (Figure 1). Two prosthetic groups are noncovalently attached to the enzyme: one is a light-harvesting photoantenna, a pterin molecule in the form of methenyltetrahydrofolate (MTHF), and the other one is the catalytic cofactor, a fully reduced deprotonated flavin molecule FADH<sup>-</sup>. The MTHF photoantenna is located in a shallow cleft between the two domains and partially sticks out from the surface of the enzyme (Figure 1).

The flavin cofactor is deeply buried and tightly surrounded by 14 amino acids within the  $\alpha$ -helical domain. It has an unusual

U-shaped conformation with the isoalloxazine and adenine rings in close proximity. The cofactor is accessible to the flat surface of the  $\alpha$ -helical domain through a hole in the middle of this domain. The hole is too small to allow the diffusion of the cofactor in and out of the enzyme but allows easy accessibility to oxygen. The hole has the right dimensions and polarity to allow the entry of the substrate, a cyclobutane pyrimidine dimer (Pyr<>Pyr) of a damaged DNA product under deep UV (200–300 nm) irradiation, as illustrated in Figure 1. Under aerobic conditions, the cofactor is oxidized into the neutral radical form FADH in most photolyases. Two photoreduction processes involving a tryptophan triad and an  $\alpha$ -helix have been proposed to convert FADH back to the biologically active form FADH<sup>-</sup> through an electron-transfer mechanism.<sup>19</sup>

During catalysis, the first step is the absorption of a photon by the antenna MTHF, which then transfers the excitation energy to the catalytic cofactor FADH<sup>-</sup> to enhance the DNA-repair efficiency.<sup>20</sup> Earlier studies<sup>12</sup> reported that the energy transfer from MTHF to FADH<sup>-</sup> takes 140–180 ps (lifetime) but occurs in less than 30 ps from MTHF to FADH. The actual time scales have not yet been determined precisely. After excitation of the active cofactor, the second elementary step in vivo is one electron transfer from the cofactor (FADH<sup>-\*</sup>) to the substrate Pyr<>Pyr. The final step is the cleavage of the cyclobutane ring of the dimer, which is believed to be ultrafast, followed by back electron transfer to restore FADH to the active form FADH<sup>-</sup>. These catalytic processes have been recently studied,<sup>15,17</sup> but the key immediate species have not yet been observed.

The flavin cofactor of the enzyme in vitro is usually oxidized to the inactive neutral radical form FADH after purification.

\* Corresponding author. E-mail: dongping@mps.ohio-state.edu. Phone: (614)292-3044. Fax: (614)292-7557.

<sup>†</sup> The Ohio State University.

<sup>‡</sup> University of North Carolina School of Medicine.

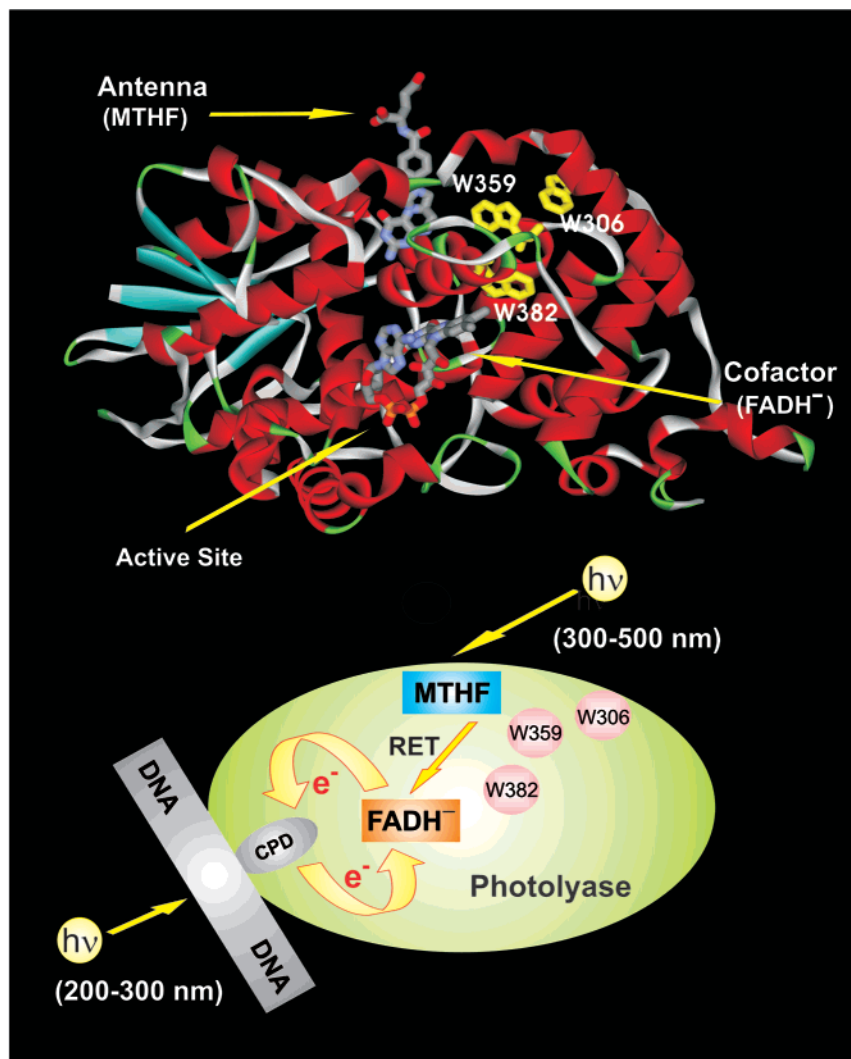


**Figure 1.** (Upper) X-ray crystal structure<sup>19</sup> of DNA photolyase from *E. coli* with the antenna molecule (MTHF), the catalytic cofactor ( $\text{FADH}^-$ ), the active site, and the tryptophan triad for the photoreduction of the oxidized neutral  $\text{FADH}$ . (Lower) Schematic representation of the overall molecular mechanism involved in the DNA repair by the photolyase enzyme. RET, resonance energy transfer. CPD, cyclobutane pyrimidine dimer ( $\text{Pyr} < > \text{Pyr}$ ).

Under illumination with visible light, the cofactor can be converted to the active form through electron transfer from neighboring aromatic residues. The residue tryptophan 306 (W306) was identified as the ultimate donor by site-specific mutagenesis, fast kinetics, and EPR analyses.<sup>13,21</sup> Two recent studies<sup>16,22</sup> reported the dynamics occurring in  $\sim 25$  ps through one electron transfer from a nearby tryptophan (W382) favoring one of the two pathways proposed on the basis of the crystal structure.<sup>19</sup> However, a steady-state photoreduction study indicated that the W382F mutant was photoreduced with 2-fold higher quantum yield relative to that of the wild type.<sup>2</sup> Clearly, more detailed work is necessary to understand both the intrachromophore energy transfer as well as the intraprotein electron transfer.

In this study, we combined femtosecond-resolved fluorescence up-conversion and transient absorption methods to determine the actual time scales of the initial resonance energy transfer from the antenna to the fully reduced and semioxidized cofactors. The photoreduction of the oxidized neutral radical cofactor  $\text{FADH}$  was carefully studied, and two reduction pathways were observed. The observed dynamics are different from those reported in previous studies.<sup>16,22</sup> Finally, the effect of oxygen in the enzyme was also examined.

The paper is organized as follows. In section II, we give our experimental setup and the sample preparation. In section III, we present the femtosecond-resolved results of the excitation-energy transfer from the antenna to the cofactor and the dynamics of photoreduction of the oxidized neutral radical cofactor  $\text{FADH}$ . Finally, the conclusion of our work is summarized in section IV.

## II. Experimental Section

All experimental measurements were carried out by using the femtosecond-resolved fluorescence up-conversion and transient absorption techniques.<sup>23</sup> The experimental setup is schematically shown in Figure 2. Specifically, the femtosecond pulse after the two-stage amplifier (Spitfire, Spectra-Physics) has a temporal width of 110 fs with an energy of more than 2 mJ and a repetition rate of 1 kHz. The laser beam is then split into two equal parts to pump two optical parametric amplifiers (OPA-800C, Spectra-Physics). For fluorescence up-conversion experiments, we used the pump wavelength at 400 nm by direct doubling of the 800-nm fundamental from the first OPA through a 0.2-mm-thick BBO crystal. The pulse energy was attenuated to 140 nJ before entering the sample cell. The fluorescence

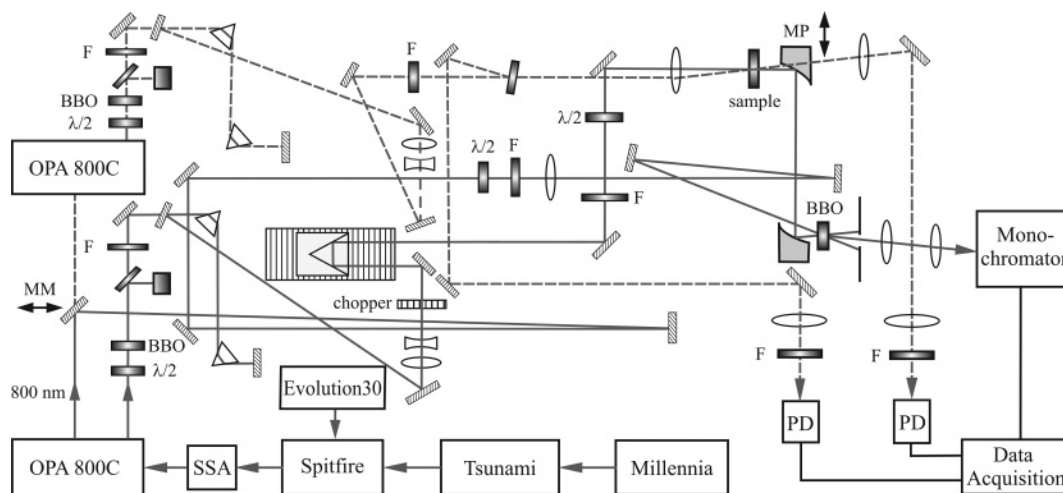


**Figure 2.** Schematic representation of the experimental setup with both the fluorescence up-conversion and the transient absorption configurations. The dashed line is for the transient-absorption probe pathway. F, filter. MM, movable mirror. MP, movable parabolic mirror. PD, photodiode. Millennium, Tsunami, Spitfire, Evolution 30, and SSA are the pump laser, femtosecond oscillator, two-stage amplifier, amplifier's pump laser, and single-shot autocorrelator, respectively.

emission was collected by a pair of parabolic focus mirrors and mixed with another fundamental pulse in a 0.2-mm BBO crystal through a noncollinear configuration. The up-converted signal from 283 to 330 nm was detected by a photomultiplier after passing through a double-grating monochromator. The response time in this noncollinear geometry is between 350 and 450 fs as determined from the up-conversion signal of Raman scattering by water in the range of 450–460 nm.

For transient absorption measurements, we used pump wavelengths of both 400 and 580 nm. The pump pulse at 580 nm was generated from a mixing of the idler (2109 nm) and the fundamental (800 nm) from the output of the first OPA through the same BBO crystal. By translating the movable mirror (MM in Figure 2) out of the laser path, the half-intensity fundamental beam (1 mJ) pumps the second OPA, and various probe wavelengths from 400 to 700 nm were generated by a mixing of the idler or signal with the fundamental. Both the pump and probe pulses were compressed through a pair of prisms with double paths to reach a temporal resolution of 60 fs. By translating the movable parabolic mirror (MP in Figure 2) out of the probe beam path, we quickly switched from fluorescence detection to transient absorption measurements. The sensitivity of the transient absorption method can reach  $10^{-4}$ – $10^{-5}$  of the absorbance change. All signals were digitized and processed by computers.

The pump beam polarization for fluorescence up-conversion experiments was set at a magic angle ( $54.7^\circ$ ) with respect to the acceptance axis of the up-conversion crystal (vertical), and the gating beam polarization was set parallel to this axis using a half-wave plate. For the transient absorption measurements, the pump beam polarization was set at a magic angle directly with respect to the probe beam, which was vertical.

The DNA photolyase from *E. coli* was prepared as described previously.<sup>24</sup> A concentration of  $\sim 300 \mu\text{M}$  was used in buffer solution at pH 7.4, containing 50 mM Tris, 50 mM NaCl, 1 mM EDTA, 10 mM DTT, and 50% (v/v) glycerol. The absorption spectrum is shown in Figure 3, and the enzyme contains the oxidized neutral radical FADH with typical absorption at wavelengths longer than 500 nm. To reduce the cofactor FADH fully, the sample was purged with nitrogen to remove oxygen and then illuminated with a high-intensity lamp with a cutoff filter to ensure that the sample was exposed at wavelengths longer than 550 nm.<sup>25</sup> The resulting fully reduced

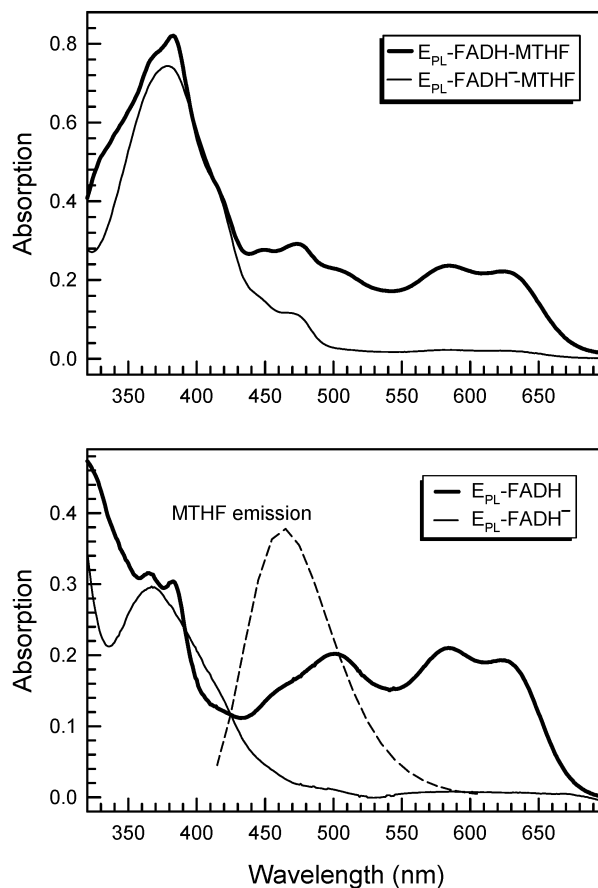


**Figure 3.** (Upper) Absorption spectra of *E. coli* photolyase in semioxidized (thick dark line) and fully reduced (thin dark line) flavin forms. (Lower) Absorption spectra of the folate-depleted enzyme with neutral radical and reduced forms of flavin. MTHF emission spectrum (dashed line) is shown to overlap with the absorption spectra of flavin, indicating resonance energy transfer from MTHF to flavin.

enzyme has absorption at  $\lambda \leq 500$  nm; see Figure 3. The absorption spectra of the folate-depleted enzyme, through the photodecomposition of MTHF by the illumination of the sample with a UV lamp at 360 nm, are also given in Figure 3.<sup>26</sup> For all experiments, all samples were kept in various rotating quartz cells to avoid heating and photobleaching.

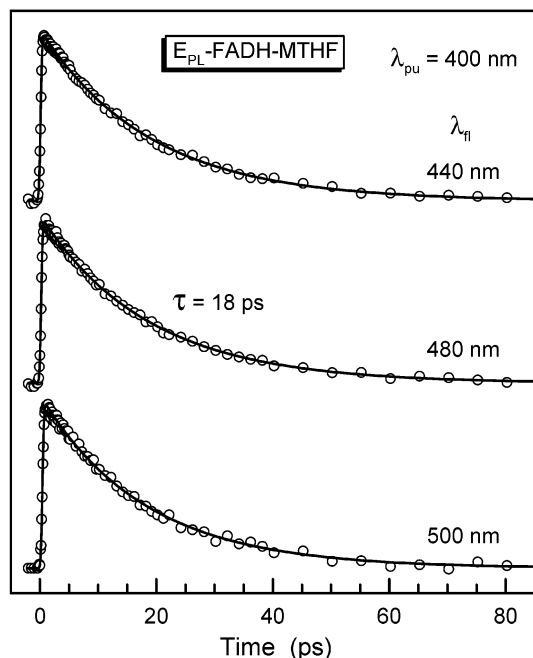


**Figure 4.** Femtosecond-resolved fluorescence transients of MTHF\* probed at several typical wavelengths. All three transients show a single-exponential decay of 18 ps. Note that the cofactor flavin is in the neutral radical form FADH.

### III. Results and Discussion

**(A) Resonance-Energy Transfer from the Folate Antenna to the Flavin Cofactor.** (a) *MTHF with the Neutral Radical Form FADH.* The femtosecond-resolved fluorescence transients of the enzyme complex  $E_{PL}$ -FADH-MTHF at 400-nm excitation under aerobic conditions are shown in Figure 4 for three typical wavelengths from the blue side to the red side. All transients were well fit by a single-exponential decay with a time constant of 18 ps. At 400-nm excitation, the MTHF absorption is dominant, and the absorption coefficient is  $\sim 25\,000\text{ M}^{-1}\text{ cm}^{-1}$  but is  $\sim 3000\text{ M}^{-1}\text{ cm}^{-1}$  for FADH.<sup>2</sup> The excitation of FADH in the enzyme results in ultrafast electron-transfer reactions with neighboring aromatic residues in less than 50 ps (see below), and the excited state (FADH\*) is basically nonfluorescent; even if it were emitting, the steady-state fluorescence profile should be at a longer wavelength than 650 nm because its absorption extends to 700 nm (Figure 2). Thus, the observed fluorescence dynamics is purely from the MTHF\* state. The fluorescence lifetime of the  $E_{PL}$ -MTHF\* complex without the flavin cofactor was reported to be 354 ps at 355-nm excitation.<sup>12</sup> Therefore, the observed dynamics of 18 ps represents the excitation-energy transfer from MTHF\* to FADH. After subtracting the population-decay contribution (354 ps), the time constant of resonance energy transfer is 19 ps, and the energy-transfer efficiency is 95%.

According to Förster energy-transfer theory, the rate of resonance energy transfer (RET) from MTHF\* to FADH depends on the relative position ( $r$ ) and orientations of donor (MTHF) and acceptor (FADH) and can be expressed as follows:

$$k_{\text{RET}} = \frac{1}{\tau_{\text{D}}} \left( \frac{R_0}{r} \right)^6 \quad (3.1)$$

$$R_0 = 9.78 \times 10^2 (\kappa^2 n^{-4} Q_{\text{D}} J)^{1/6} \quad (3.2)$$

$R_0$  (in nm), the critical transfer distance, is defined as the donor-acceptor distance at which the transfer efficiency is 50%.  $\kappa^2$  is

the orientation factor,  $n$  is the refractive index of the medium ( $\sim 1.4$ ),  $\tau_{\text{D}}$  and  $Q_{\text{D}}$  are the donor excited-state lifetime and quantum yield in the absence of the acceptor, respectively, and  $J$  is the spectral overlap integral (in  $\text{cm}^3 \cdot \text{M}^{-1}$ ) between donor emission and acceptor absorption. The X-ray structure reported a distance ( $r$ ) of 16.8 Å between MTHF and FADH.<sup>19</sup> With  $\tau_{\text{D}} = 354\text{ ps}$ , the derived  $R_0$  is 27.35 Å. Given that  $Q_{\text{D}} = 0.32$  and  $J = 2.06 \times 10^{-14}\text{ cm}^3 \cdot \text{M}^{-1}$ ,<sup>12</sup> we obtained a value of 0.28 for the orientation factor  $\kappa^2$ . This low value is consistent with the observed unfavorable orientations of two chromophores in the X-ray structure. The poor alignment of the two molecules may be due to the structural constraints from retaining three functional binding sites (MTHF, FADH, and the substrate DNA). High energy-transfer efficiency by favorable orientations with a larger orientation factor has been observed in another class of photolyases.<sup>27</sup>

The observed single 18-ps exponential decay is independent of fluorescence wavelength detection. Thus, in buffer solution with 50% (v/v) glycerol, the solvation process of MTHF\* in the enzyme makes negligible contributions to the observed energy-transfer dynamics. The hydration dynamics on protein surfaces has been recently observed on the time scale of tens of picoseconds using intrinsic tryptophan as a local optical probe.<sup>28–35</sup> In rubredoxin, the resonance energy-transfer process from the excited W3/W36 to the Fe-S cluster is convoluted with the hydration dynamics of tryptophan, and both occur in  $\sim 15\text{ ps}$ .<sup>28</sup> In human thioredoxin, the electron-transfer dynamics from the excited W31 to the disulfide bond (S-S) mixes with the tryptophan hydration process, and both also occur in  $\sim 20\text{ ps}$ .<sup>35</sup> In those systems, we typically observed fluorescence wavelength-dependent transients, and the dynamics systematically slow from the blue side to the red side. Here, we observed similar transients for all fluorescence wavelengths, indicating that the chromophore MTHF is buried in the shallow cleft between the two domains and the solvation dynamics, if any, would be much longer than the observed energy-transfer process of 18 ps.

As shown below, the excited FADH proceeds through ultrafast electron transfer with neighboring aromatic residues to form the fully reduced FADH<sup>-</sup>. However, the signal in Figure 4 showed no changes for relatively long-time irradiation by laser pulses in our experiments, indicating the efficient reaction cycling of FADH during the pulse interval (2 ms with the chopper). Thus, in the presence of oxygen the FADH<sup>-</sup> could be oxidized back to FADH in less than 2 ms. In Figure 5, we show the fluorescence transients gated at 530-nm emission in the presence and absence of O<sub>2</sub>. With O<sub>2</sub> (Figure 5a), the transient gave the same energy-transfer dynamics of 18 ps. Without O<sub>2</sub> (Figure 5b), a new component of 160 ps (20%) started to appear. As the irradiation continued, the percentage of the 160-ps component (65%) increased, and that of the 18-ps component (35%) decreased, as shown in Figure 5c. These observations show that without O<sub>2</sub> the FADH<sup>-</sup> could not be oxidized to FADH in 2 ms. Thus, the observed 160 ps results from resonance energy transfer from MTHF\* to the fully reduced FADH<sup>-</sup>, in agreement with previous measurements.<sup>12</sup> Recent studies<sup>16,22</sup> also showed that it takes more than 10 ms to finish the reoxidation of FADH<sup>-</sup> under anaerobic conditions.

(b) *MTHF with the Fully Reduced Active Form FADH<sup>-</sup>.* To confirm the observed energy transfer between MTHF and FADH<sup>-</sup>, we fully reduced FADH to FADH<sup>-</sup> by irradiation of the sample with visible light ( $\lambda \geq 550\text{ nm}$ ) under anaerobic conditions;<sup>25</sup> see Figure 3. Figure 6 shows the femtosecond-resolved fluorescence transient gated at 440-nm emission. The

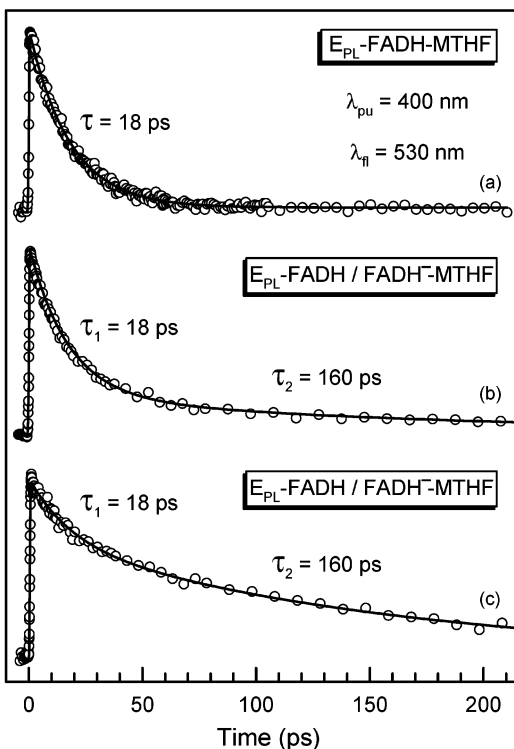


**Figure 5.** Femtosecond-resolved fluorescence transients probed at 530 nm under (a) aerobic conditions (with  $O_2$ ), (b) anaerobic conditions (no  $O_2$ ), and (c) anaerobic conditions with longer-time data collection; see text. The 18- and 160-ps dynamics represent the  $MTHF^*\text{-FADH}$  and  $MTHF^*\text{-FADH}^-$  energy transfers, respectively.

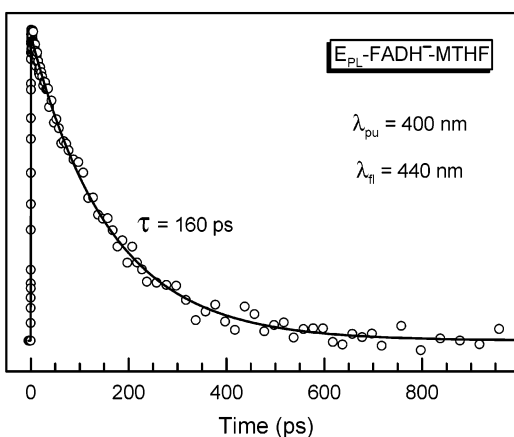


**Figure 6.** Femtosecond-resolved fluorescence transient of the  $MTHF^*$  decay probed at 440 nm. The transient follows a single-exponential decay of 160 ps. Note that the cofactor flavin is in the fully reduced form  $FADH^-$ .

signal is best fit by a single-exponential decay of 160 ps, consistent with the result obtained at 530-nm emission. The excitation of  $FADH^-$  ( $\sim 4000\text{ M}^{-1}\text{ cm}^{-1}$ ) gives a weak emission that peaks at 505 nm but no emission at 440 nm. Thus, the observed transient at 440 nm is purely from the  $MTHF^*$  state, and the observed 160 ps does represent the energy-transfer process from  $MTHF^*$  to  $FADH^-$ . After considering the population-decay contribution (354 ps), the resulting time constant of resonance energy transfer is 292 ps, and the energy-transfer efficiency is only 55%.

According to eq 3.1, the resulting  $R_0$  for  $MTHF\text{-FADH}^-$  energy transfer is 17.35 Å. Using eq 3.2 and  $J = 0.34 \times 10^{-14}\text{ cm}^3\text{M}^{-1}$ ,<sup>12</sup> we derived a value of 0.11 for the orientation factor  $\kappa^2$ , which is smaller than the one (0.28) obtained for the relative

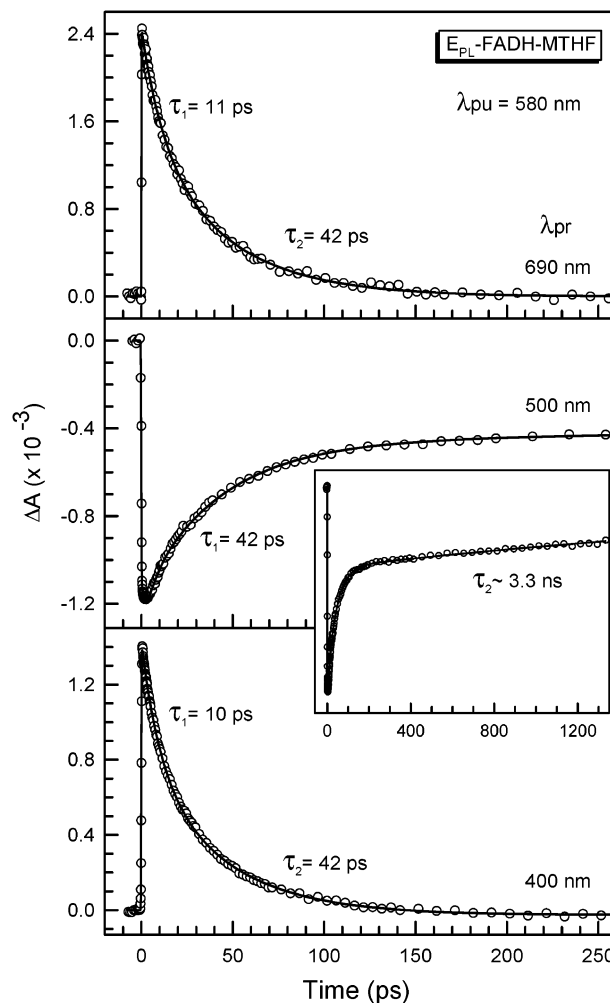


**Figure 7.** Femtosecond-resolved transient absorption measurements probed at 690 nm (top), 500 nm (middle), and 400 nm (bottom). The excitation wavelength is at 580 nm, and only the  $FADH$  molecules were excited. The signal in the long-time range (more than 1 ns) probed at 500 nm is shown in the inset.

$MTHF\text{-FADH}$  orientations. After the reduction of the neutral  $FADH$ , the negatively charged flavin cofactor  $FADH^-$  may optimize electrostatic interactions with neighboring charged residues such as R344 and D372 and stacking interactions with aromatic residues such as W277, resulting in the orientation change that we observed here. Otherwise, if we assume the same orientation factor of 0.28 as for  $FADH$ , we would obtain a spectral overlap integral of  $0.13 \times 10^{-14}\text{ cm}^3\text{M}^{-1}$  for  $MTHF\text{-FADH}^-$  energy transfer.

We also observed that over long irradiation of the sample by laser pulses the signal in Figure 6 gradually decreased but the overall shape remained the same. This is due to the photodecomposition of  $MTHF$  caused by one electron transfer from the excited  $FADH^-$ , as reported before.<sup>26</sup>

**(B) Electron-Transfer Dynamics of the Cofactor Reduction.** (a) *Two Electron-Transfer Pathways.* To understand the electron-transfer (ET) mechanism of  $FADH$  photoreduction, we performed a series of transient absorption measurements to observe the ET state and the ground-state recovery of  $FADH$ . Figure 7 gives three typical transients probed in the range of 400–690 nm. At 580-nm excitation, only  $FADH$  was excited, and  $MTHF$  had no absorption. Specifically, at 690 nm we observed only a decay signal, and thus the  $FADH^*$  dynamics was dominant. The ET products of  $FADH^-$  and  $W^+$ , if the

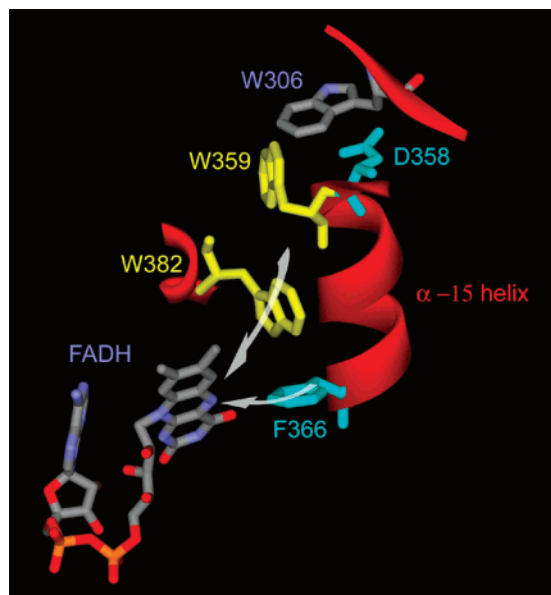


**Figure 8.** Potential electron-transfer pathways for neutral cofactor photoreduction:<sup>19</sup> Excited FADH can be reduced by one electron hop from either the amino acid residue W382 or F366 as shown by the arrows. One route passes along the tryptophan triad (W382 ← W359 ← W306), and the other one evolves after the initial electron hop along the  $\alpha$ -15 helix through the electron tunneling (F366 ←  $\alpha$ -helix ← W306) or by the electron hopping through the tryptophan triad again (F366 ← W382 ← W359 ← W306).

electron donor is tryptophan, have no absorption at 690 nm. The transient was best fit by a double-exponential decay with two time constants of 11 ps (36%) and 42 ps (64%), respectively. At 500 nm, we observed an initial bleaching and a formation/recovery signal. Thus, the absorptions of the ET states and the ground-state FADH were dominant. The transient can be best fit with two time constants of 42 ps (60%) and  $\sim$ 3.3 ns (40%) if the signal returns to zero. We did not observe any contributions from the 11-ps component as observed at 690 nm. When the probe wavelength was tuned to 400 nm, we observed a positive decay signal, and thus the FADH\* dynamics dominated again. The transient has similar dynamics to that observed at 690 nm with the two time constants of 10 ps (42%) and 42 ps (58%).

Previous site-specific mutagenesis<sup>21</sup> identified W306 as the ultimate electron donor for the flavin photoreduction. On the basis of the crystal structure, two potential electron-transfer pathways of the FADH photoreduction were proposed:<sup>19</sup> one passes through a tryptophan triad (W382 ← W358 ← W306) with three electron hops, and the other route to W306 consists of an  $\alpha$ -helix ( $\alpha$ -15) between residues F366 and D358 through electron tunneling; see Figure 8. It was recently reported<sup>16,22</sup> that photoreduction exhibits a single-exponential decay of 24 ps for the FADH\* dynamics, and this was attributed to electron transfer from W382 (Figure 8) to FADH\* to form W382<sup>+</sup> and FADH<sup>-</sup>. This process was then followed by two subsequent electron hops from W358 and W306 in less than 10 ns for each. These observations favored the electron-hopping pathway. However, steady-state photoreduction measurements with the W382F mutant gave results inconsistent with this model.<sup>2</sup> In contrast to the time-resolved transient absorption measurements<sup>22</sup> that indicated a nearly complete turn off of the photoreduction, the quantum yield measurements by steady-state irradiation revealed a 2-fold enhancement of photoreduction,<sup>2</sup> which favored an electron tunneling mechanism, also supported by quantum calculations.<sup>36</sup>

The double-exponential decay of the electron-transfer dynamics from aromatic residues to flavin has also been observed in other flavoproteins such as riboflavin-binding protein,<sup>37</sup> glucose oxidase,<sup>37,38</sup> and flavodoxin.<sup>39</sup> These double decays were attributed to the multiple neighboring electron donors of aromatic residues (W, Y, or F) accompanying the local dynamic heterogeneous configurations. Here, the observed double-exponential decay of FADH\* in photolyase also reflects the dynamic heterogeneity of local structures, resulting in two electron-transfer pathways: electron hopping through the tryptophan triad with the initial electron jump from W382 in  $\sim$ 10 ps and electron tunneling through the  $\alpha$ -15 helix with the initial electron separation through F366 in  $\sim$ 40 ps. The edge-to-edge distance of the rings between F366 and FADH is 4 Å. The electron hop from W382 is faster because of the favored redox potentials (W/W<sup>+</sup> vs F/F<sup>+</sup>), although the separation is larger (4.2 Å). The observed initial two electron-transfer pathways are also strongly supported by the transient probed at 500 nm (Figure 7); we observed only the 42-ps component and did not observe the 11-ps contribution. The absence of the 11-ps dynamics is due to the weak absorption of FADH\* and W382<sup>+</sup> ( $\sim$ 1000 M<sup>-1</sup>cm<sup>-1</sup> at 500 nm), whereas for the tunneling pathway we could detect the F366<sup>+</sup> formation because it has an absorption maximum ( $\sim$ 3000–4000 M<sup>-1</sup> cm<sup>-1</sup>) at  $\sim$ 500 nm.<sup>40,41</sup> The observed 3.3-ns dynamics at 500 nm reflects the recovery process of FADH either by back electron transfer or through oxygen reduction.

(b) *Photoreduction through Folate Light Harvesting.* To further confirm the observed two initial electron-transfer pathways, we tuned the pump wavelength to 400 nm to dominantly excite MTHF. Figure 9 shows two transients probed at 690 and 500 nm. As we observed above, the excitation-energy transfer from MTHF\* to FADH takes 18 ps, and the electron transfer of the flavin FADH reduction proceeds along two pathways with 11 and 42 ps. Thus, for the electron-hopping route, because the FADH\* decay (11 ps) is faster than its formation (18 ps), the FADH\* molecules could not be easily accumulated, and we should also observe an *apparent* formation signal of 11 ps. At 690 nm, we did observe a formation signal of 11 ps (–18%) and a dominant decay component of 42 ps (100%). Thus, the overall signal in the range of 0–10 ps appeared to be flat because of the signal superposition of the 11-ps formation and the 42-ps decay; see the inset in Figure 9. We did not observe any 18-ps dynamics at this wavelength, indicating the overall cancellation of the signal decay and formation (MTHF\* and FADH\*). These observations are striking and convincing and elucidate the two initial parallel photoreduction pathways through W382 and F366 sampled by the local dynamic configurations. When the probe wavelength was tuned to 500 nm, we observed a strong positive signal, and the transient was best represented by a single-exponential decay of 18 ps, equal to the observed energy-transfer dynamics and consistent with the fluorescence up-conversion measurement. This result shows the dominant absorption of MTHF\* at 500 nm.

It should be pointed out here that site-specific mutagenesis studies<sup>2</sup> of W382A showed the complete elimination of photoreduction pathways. Those studies indicated that W382 is a structurally and chemically important residue. The mutation not only eliminates the electron-hopping pathway through the tryptophan triad but probably also changes the local structure and shuts off the initial step of the tunneling route. Another scenario is that after the initial electron transfer from F366 to FADH\* the electron tunneling (or hole migration) does not

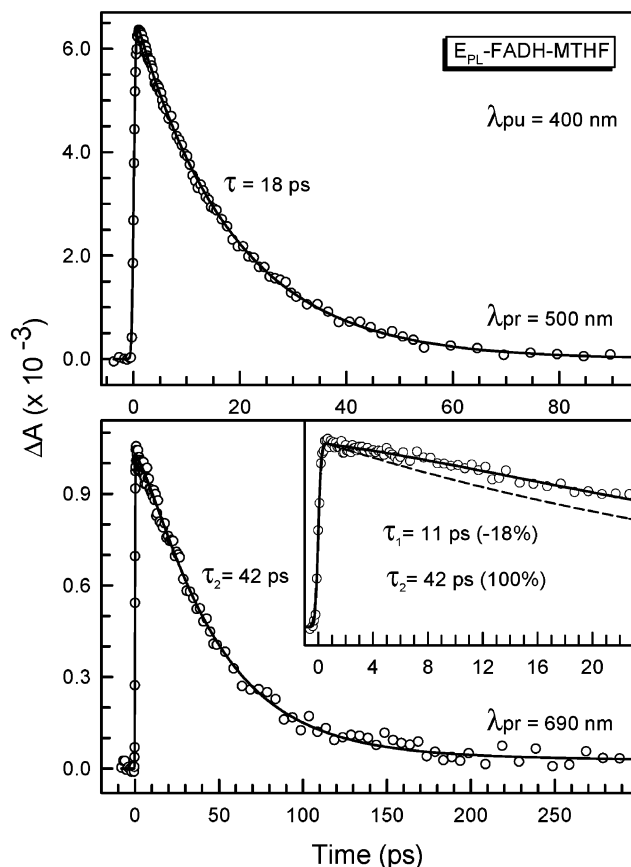


**Figure 9.** Femtosecond-resolved transient absorption measurements with excitation at 400 nm. (Lower) At the probe wavelength of 690 nm, the transient is best fit by an 11-ps formation component and a 42-ps decay contribution. Note that the flat signal in the 0–10-ps range in the inset is due to the superposition of these two components. The dashed line is the pure 42-ps decay shown for comparison. (Upper) At the 500-nm probe, the MTHF\* dynamics dominates with a single-exponential decay of 18 ps, consistent with the fluorescence up-conversion result shown in Figure 4.

follow the  $\alpha$ -15 helix but instead evolves along the tryptophan triad again. The X-ray structure shows a close distance of 3.8 Å between F366 and W382. Clearly, more femtosecond-resolved experiments of mutated enzymes are needed to resolve these electron-transfer processes fully, especially the mutation of F366.

(c) *Lifetime of the Excited FADH<sup>-</sup>*. We also performed measurements of DNA photolyase with the fully reduced state under anaerobic conditions. The femtosecond-resolved transient absorption is shown in Figure 10 with excitation at 400 nm and a probe at 500 nm. The dynamics is best represented by a double-exponential decay with two time constants of 160 ps (52%) and 760 ps (48%). The 160-ps component, the decay of MTHF\*, represents the excitation-energy transfer from MTHF\* to FADH<sup>-</sup>, consistent again with the fluorescence up-conversion result. The observed 760 ps is the lifetime of the excited FADH<sup>-</sup>, in excellent agreement with the fluorescence up-conversion measurement of the FADH<sup>-</sup>\* decay in the MTHF-depleted enzyme, which is also shown in Figure 10.

#### IV. Conclusions

In this contribution, we report our first studies of the complex protein dynamics on DNA photolyase with femtosecond resolution. We combined both femtosecond fluorescence up-conversion and transient absorption methods to dissect the elementary steps involved in resonance energy transfer by photoantenna

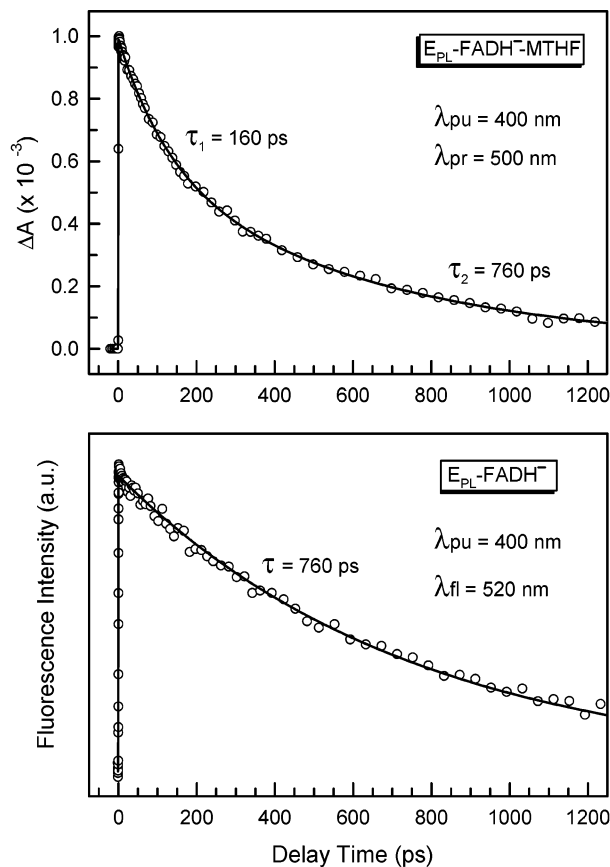


**Figure 10.** (Upper) Femtosecond-resolved transient absorption detection of the fully reduced enzymes under anaerobic conditions at an excitation of 400 nm and a probe of 500 nm. The first decay component (160 ps) represents the energy transfer from MTHF\* to FADH<sup>-</sup>, consistent with the fluorescence up-conversion result as shown in Figure 6. The other component of 760 ps is the lifetime of FADH<sup>-</sup>\* in the enzyme. (Lower) Femtosecond-resolved fluorescence up-conversion signal of FADH<sup>-</sup>\* in the MTHF-depleted enzyme gated at 520-nm emission with 400-nm excitation. The transient gives a 760-ps lifetime of FADH<sup>-</sup>\*, in excellent agreement with the transient-absorption result in the upper panel.

initiation and electron transfer by photoreduction of the flavin neutral cofactor. The molecular mechanism and the measured dynamics are summarized in Figure 11. Specifically, we elucidated the following important processes:

(1) The dynamics of excitation-energy transfer from the antenna molecule to the cofactor was determined from both fluorescence detection and transient-absorption measurements consistently: 292 ps for the physiologically relevant cofactor FADH<sup>-</sup> and 19 ps for the *in vitro* oxidized cofactor FADH. The derived orientation factors are 0.11 for the MTHF–FADH<sup>-</sup> pair and 0.28 for MTHF–FADH.

(2) The physiological form of the enzyme contains the flavin in two electron reduced FADH<sup>-</sup> form,<sup>42</sup> and the nonphotoreducible mutants are as active as the wild-type enzyme,<sup>21</sup> indicating that the photoreduction of FADH, which is generated *in vitro* during purification, may not be directly relevant to the action mechanism. Nevertheless, photolyase does provide an excellent system for the study of mechanisms of intraprotein electron transfer. Our results show that the dynamics of the FADH photoreduction, either through excitation-energy transfer from MTHF\* or by direct excitation, evolve along two electron-transfer pathways to reach the final electron donor W306: one involves a tryptophan triad by the initial electron hop from W382 in  $\sim$ 10 ps, and the other route starts with the initial electron

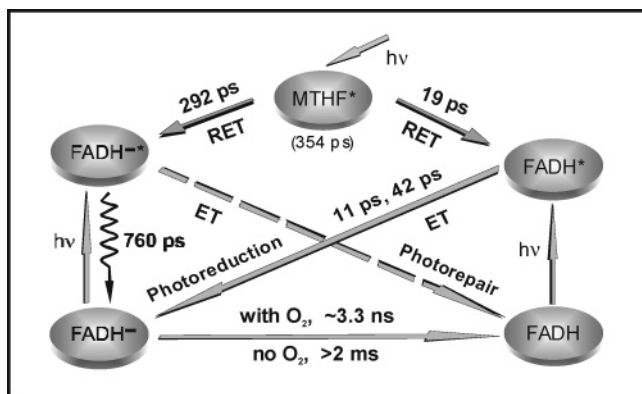


**Figure 11.** Schematic representation of the molecular mechanism and the measured dynamics of energy transfer of the antenna initiation and of electron transfer of the neutral cofactor reduction. The dashed line represents the DNA-repair pathway with one electron transfer from the biologically active cofactor  $\text{FADH}^{\bullet\bullet}$  to the damaged  $\text{Pyr} \leftrightarrow \text{Pyr}$  as shown in Figure 1.

separation through F366 in 40 ps followed by either the tunneling along the  $\alpha$ -15 helix or the hopping through the tryptophan triad again.

(3) The dynamics of the  $\text{FADH}^{\bullet\bullet}$  reoxidation after photoreduction under aerobic conditions occurs in several nanoseconds ( $\sim 3.3$  ns) either through back electron transfer or oxygen reduction. In the absence of oxygen, the fully reduced cofactor takes milliseconds to be reoxidized.

In summary, the results reported here reveal significant details of the nature of the ultrafast dynamics in DNA photolyase and lay a solid foundation for further studies of mapping out the entire DNA-repair process. The structure and dynamics of photolyase are beautifully intertwined to funnel energy along the functional coordinate. During these processes, ultrafast dynamics is necessary to reach high biological efficiency.<sup>43,44</sup> Femtosecond methods are ideal and powerful enough to reveal the actual dynamics and molecular mechanism on the local atomic scale as shown here in DNA photolyase.

**Acknowledgment.** This work was supported by the Selective Investment of The Ohio State University through the Biophysics Initiative in the Physics Department (D.Z.) and an NIH grant 31082 (A.S.). We thank Professor Ahmed Zewail (Caltech) for his constant encouragement. We also thank Dr. Haiyu Wang for valuable discussions, Dr. Lale Dawut for purifying photolyase, and Jongjoo Kim and Lijuan Wang for their help during experiments.

## References and Notes

- (1) Begley, T. P. *Acc. Chem. Res.* **1994**, *27*, 394.
- (2) Sancar, A. *Chem. Rev.* **2003**, *103*, 2203.
- (3) Sancar, G. B. *Mutat. Res.* **1990**, *236*, 147.
- (4) Kim, S. T.; Sancar, A. *Photochem. Photobiol.* **1993**, *57*, 895.

- (5) Taylor, J. S. *Acc. Chem. Res.* **1994**, *27*, 76.
- (6) Sancar, A. *Biochemistry* **1994**, *33*, 2.
- (7) Heelis, P. F.; Hartman, R. F.; Rose, S. D. *Chem. Soc. Rev.* **1995**, *24*, 289.
- (8) Todo, T. *Mutat. Res.* **1999**, *434*, 89.
- (9) Deisenhofer, J. *Mutat. Res.* **2000**, *460*, 143.
- (10) Sancar, A. *Annu. Rev. Biochem.* **2000**, *69*, 31.
- (11) Okamura, T.; Sancar, A.; Heelis, P. F.; Begley, T. P.; Hirata, Y.; Mataga, N. *J. Am. Chem. Soc.* **1991**, *113*, 3143.
- (12) Kim, S. T.; Heelis, P. F.; Okamura, T.; Hirata, Y.; Mataga, N.; Sancar, A. *Biochemistry* **1991**, *30*, 11262.
- (13) Kim, S. T.; Sancar, A.; Essenmacher, C.; Babcock, G. T. *Proc. Natl. Acad. Sci. U.S.A.* **1993**, *90*, 8023.
- (14) Langenbacher, T.; Zhao, X.; Bieser, G.; Heelis, P. F.; Sancar, A.; Michel-Beyerle, M. E. *J. Am. Chem. Soc.* **1997**, *119*, 10532.
- (15) Gindt, Y. M.; Vollenbroek, E.; Westphal, K.; Sackett, H.; Sancar, A.; Babcock, G. T. *Biochemistry* **1999**, *38*, 3857.
- (16) Aubert, C.; Vos, M. H.; Mathis, P.; Eker, A. P. M.; Brettel, K. *Nature* **2000**, *405*, 586.
- (17) MacFarlane, W. A.; Stanley, R. J. *Biochemistry* **2003**, *42*, 8558.
- (18) Schelvis, P. M. J.; Ramsey, M.; Sokolova, O.; Tavares, C.; Cecala, C.; Connell, K.; Wagner, S.; Gindt, Y. M. *J. Phys. Chem. B* **2003**, *107*, 12352.
- (19) Park, H.; Kim, S.; Sancar, A.; Deisenhofer, J. *Science* **1995**, *268*, 1866.
- (20) Payne, G.; Sancar, A. *Biochemistry* **1990**, *29*, 7715.
- (21) Li, Y. F.; Heelis, P. F.; Sancar, A. *Biochemistry* **1991**, *30*, 6322.
- (22) Byrdin, M.; Eker, A. P. M.; Vos, M. H.; Brettel, K. *Proc. Natl. Acad. Sci. U.S.A.* **2003**, *100*, 8676.
- (23) Lu, W.; Zhong, D. To be submitted for publication.
- (24) Sancar, A.; Smith, F. W.; Sancar, G. B. *J. Biol. Chem.* **1984**, *259*, 6028.
- (25) Heelis, P. F.; Sancar, A. *Biochemistry* **1986**, *25*, 8163.
- (26) Heelis, P. F.; Payne, G.; Sancar, A. *Biochemistry* **1987**, *26*, 4634.
- (27) Kim, S. T.; Heelis, P. F.; Sancar, A. *Biochemistry* **1992**, *31*, 11244.
- (28) Zhong, D.; Pal, S. K.; Zhang, D.; Chan, S. I.; Zewail, A. H. *Proc. Natl. Acad. Sci. U.S.A.* **2002**, *99*, 13.
- (29) Pal, S.; Peon, J.; Zewail, A. H. *Proc. Natl. Acad. Sci. U.S.A.* **2002**, *99*, 1763.
- (30) Peon, J.; Pal, S.; Zewail, A. H. *Proc. Natl. Acad. Sci. U.S.A.* **2002**, *99*, 10964.
- (31) Pal, S. K.; Peon, J.; Bagchi, B.; Zewail, A. H. *J. Phys. Chem. B* **2002**, *106*, 12376.
- (32) Pal, S.; Peon, J.; Zewail, A. H. *Proc. Natl. Acad. Sci. U.S.A.* **2002**, *99*, 15297.
- (33) Zhao, L.; Pal, S. K.; Xia, T.; Zewail, A. H. *Angew. Chem., Int. Ed.* **2004**, *43*, 60.
- (34) Lu, W.; Kim, J.; Qiu, W.; Zhong, D. *Chem. Phys. Lett.* **2004**, *388*, 120.
- (35) Qiu, W.; Zhong, D. To be submitted for publication.
- (36) Cheung, M. S.; Daizadeh, I.; Stuchebrukhov, A. A.; Heelis, P. F. *Biophys. J.* **1999**, *76*, 1241.
- (37) Zhong, D.; Zewail, A. H. *Proc. Natl. Acad. Sci. U.S.A.* **2001**, *98*, 11867.
- (38) Mataga, N.; Chosrowjan, H.; Shibata, Y.; Tanaka, F.; Nishina, Y.; Shiga, K. *J. Phys. Chem. B* **2000**, *104*, 10667.
- (39) Mataga, N.; Chosrowjan, H.; Taniguchi, S. *J. Phys. Chem. B* **2002**, *106*, 8917.
- (40) Shida, T. *Electronic Absorption Spectra of Radical Ions*; Elsevier: Amsterdam, 1988.
- (41) Shida, T.; Hamill, W. *J. Chem. Phys.* **1966**, *44*, 2375.
- (42) Payne, G.; Heelis, P. F.; Rohrs, B. R.; Sancar, A. *Biochemistry* **1987**, *26*, 7121.
- (43) Wang, Q.; Schoenlein, R. W.; Peteanu, L. A.; Mathies, R. A.; Shank, C. V. *Science* **1994**, *266*, 422.
- (44) Chosrowjan, H.; Taniguchi, S.; Mataga, N.; Unno, M.; Yamauchi, S.; Hamada, N.; Kumauchi, M.; Tokunaga, F. *J. Phys. Chem. B* **2004**, *108*, 2686.